2019 Smart Grid Conference (SGC)

A Distributed Control Strategy with Fractional Order PI Controller for DC Microgrid

Mehdi Doostinia
Faculty of Electrical and Computer Engineering
Tarbiat Modares University
Tehran, Iran
m.doostinia@modares.ac.ir

Mohammad.T H.Beheshti
Faculty of Electrical and Computer Engineering
Tarbiat Modares University
Tehran, Iran
mbehesht@modares.ac.ir

Seyed Amir Alavi
School of Electronic Engineering and Computer Science
Queen Mary University of London
London E1 4NS, UK
s.alavi@qmul.ac.uk

***Abstract*—This paper presents a novel distributed consensus control strategy for stabilization of the buses voltages and energy balancing of the storage in DC microgrids. The proposed strategy works based on sparse communication graph in which the agents possess fractional order proportional integral (FOPI) dynamics. The FOPI controller is used for energy balancing energy storage (ES) systems and to regulate the average DC microgrid buses voltages. The proposed control strategy operates in both operation modes of DC microgrid: 1) islanded mode, -2) grid connected mode. In both modes the average voltage of DC microgrid converges to the microgrid desire reference voltage. The energy storages systems are controlled independently of the operating mode to achieve and maintain a balanced energy level. The simulation results demonstrate the performance of the control strategy in a case study of a 10 bus 380 V DC with intermittent photovoltaic generation.**

***Index Terms*— Consensus control, DC microgrid, distributed control strategy, Fractional order PI control.**

I. INTRODUCTION

DC microgrids have gained wide acceptance and significant acceleration in distribution power systems. This is because they provide several advantages over their AC counterparts such as eliminating the AC/DC conversion steps and not have reactive power, which leads to the reduction in energy loss and further economic savings [1], [2].

Three well-known control strategies for microgrid are [3]:

- Centralized
- Decentralized
- Distributed

In centralized control strategy, all data should be collected by a central controller. Therefore, the computational complexity is increased and the system exposes a single point of failure that leads to reduced reliability of the system. In decentralize control strategy, each controller operates based on only the local information. In this strategy, there are a set of controllers in the microgrid such as distributed generation (DG) controllers, converter controllers and load controllers. There is no direct communication between controllers. This strategy has disadvantages such as steady state voltage offset and inadequate response time for load variation, which leads to instability of the microgrid [4]. In distributed control strategies, autonomous agents use local information and neighbor-to-neighbor communication over a sparse communication network to achieve cooperative objectives [5]. Distributed control strategy improves the system performance compared to decentralized control as well as the central control. This strategy has advantages such as robustness, scalability, high flexibility, reduction in computational complexity, no single point of failure and distribution of the tasks among the local controllers in the DC microgrid [6], [7].

In recent years, due to the advent of fractional calculus, the classical models, which were based on integer order derivatives have been replaced with models that are using fractional order integrator. In this regard, the number of its applications has been rapidly grown [8], [9].

Fractional order PID (FOPID) has higher freedom degree for the existence of two extra adjustable parameters (λ, μ). Therefore, a wide range of parameters are available to control the target [10].

In this paper we present a novel distributed control strategy with fractional order PI controller agents. The voltage of buses and the energy per-unit level of the ES systems are controlled in a distributed manner. After the distributed average consensus protocol, the FOPI controller is applied as the feedback signal to control the converters output. The voltage of buses and the energy per-unit level of the ES systems are controlled in a distributed manner.

978-1-7281-5894-5/19/$31.00 ©2019 IEEE

Authorized licensed use limited to: Queen Mary University of London. Downloaded on November 05,2020 at 13:08:23 UTC from IEEE Xplore. Restrictions apply.

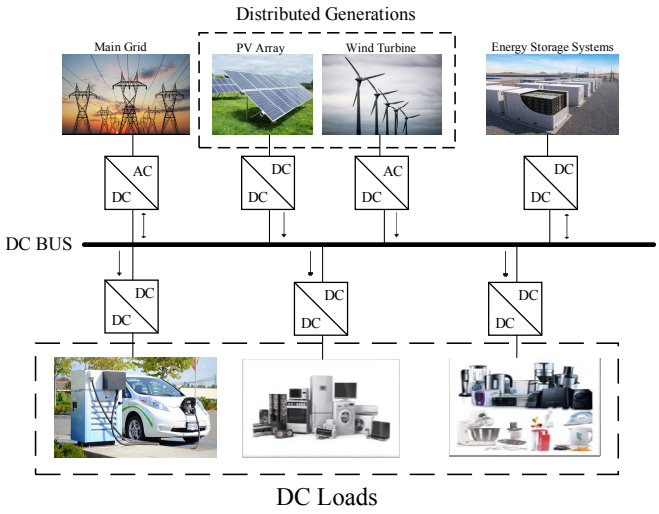

Figure 1. DC microgrid with its component.

The voltage of buses and the energy per-unit level of the ES systems are controlled in a distributed manner. After the distributed average consensus protocol, the FOPI controller is applied as the feedback signal to control the converters output. Finally, the converters stabilize the voltage of the buses. The effectiveness of the proposed method is verified by the simulation using Matlab Simulink software to control the buses voltage of the DC microgrid.

The rest of the paper is organized as follows. First, in section II the DC microgrid and its components are described. In section III an introduction of fractional calculus and fractional order PID controller discussed. In section IV, distributed average consensus protocol is illustrated. In section V, the distributed control strategy is presented. In section VI, the case study DC microgrid is described. In section VII, the simulation results are provided. Finally, in section VIII, the conclusion are drawn.

II. DC MICROGRID

In general, a DC microgrid consist of four main components. These components are DGs, power converters, ES systems and loads. DGs include PV generations or wind turbines, the converters are DC-DC and DC-AC and the usually used devices for ES systems consist of flywheel, electromechanical batteries and super capacitor. These are easily implemented in the DC microgrid for their inherent DC output. Load fluctuation causes the fast voltage dynamics and the main task of ES systems are to compensate this fast voltage dynamics. DC microgrid with general configuration have shown in Fig 1. DC microgrid are generally consist of two islanded mode and connection to the grid mode. In this paper our simulation includes both two operation mode.

In this research for distributed energy resources for example PV used of a maximum power point tracking (MMPT) scheme. Meaning that the PV working with 100% of its capacity.

III. FRACTIONAL ORDER CONTROLLER

A. *Introduction of Fractional Calculus*

The fractional calculus is an extension of integration and differentiation to non - integer order operators ${}_a\mathfrak{D}_t^\alpha$. Where the limits of operation denoted by t and a [8]. The continuous integro-differential operator of order $\alpha\epsilon\mathbb{R}^+$ is defined in the following way:

$$ {}_a\mathfrak{D}_t^\alpha = \begin{cases} d^\alpha/dt^\alpha & , \alpha > 0 \\ 1 & , \alpha = 0 \\ \int_\alpha^t (d\tau)^{-\alpha} & , \alpha < 0 \end{cases} \quad (1) $$

In fractional calculus the basic functions is Euler's Gamma function which is defined by:

$$ \Gamma(z) = \int_0^\infty e^{-t} t^{z-1} \quad (2) $$

which converges in the right half of the complex plane, $R(z) > 0$.

Some definitions of fractional differ-integral are provided. Three well-known definition of them are the Riemann_Liouville, Caputo definitions and Grünwald-Letnikov.

The Riemann-Liouville integro-differential is a commonly used definition [9] and it is as follows:

$$ {}_a\mathfrak{D}_t^\alpha = f(t) = \frac{1}{\Gamma(m-\alpha)} \left(\frac{d}{dt}\right)^m \int_\alpha^t \frac{f(\tau)}{(t-\tau)^{\alpha-m+1}} d\tau \quad (3) $$

for $m-1 < \alpha < m, m\epsilon N$, where $\Gamma(.)$ is Euler's gamma function.

The Grünwald-Letnikov definitions as follow:

$$ {}_a\mathfrak{D}_t^\alpha = f(t) = \lim_{h\to 0} \frac{1}{h^\alpha} \sum_{j=0}^k (-1)^j \binom{\alpha}{j} f(t-jh) \quad (4) $$

Where $a = 0,\ t = kh,\ k$ is the number of steps, and h is the step size.

The Caputo fractional derivative of order α of a continuous function $f: R^+ \to R$ is defined as follows [11]:

$$ {}_a\mathfrak{D}_t^\alpha = \begin{cases} \frac{1}{\Gamma(m-\alpha)} \int_\alpha^t \frac{f^{(m)}(\tau)}{(t-\tau)^{\alpha-m+1}} d\tau & , m-1 < \alpha < m \\ \frac{d^m}{dt^m} f(t) & , \alpha = m \end{cases} \quad (5) $$

Where m is the first integer larger than α.

As we know the Laplace transform of α-th derivative with $\alpha\epsilon\mathbb{R}^+$ of $x(t)$ relaxed at $t = 0$ with the assuming zero initial condition is given by:

$$ \int_0^\infty e^{-st} {}_0\mathfrak{D}_t^\alpha f(t) dt = s^\alpha F(s) \quad (6) $$

Where $S = j\omega$ is Laplace transform variable.

Therefore, transfer function form in Laplace domain of a fractional-order differential equation can be write as follows:

$$ G(s) = \frac{b_m s^{\beta m} + b_{m-1} s^{\beta m-1} + \cdots + b_0 s^{\beta_0}}{a_n s^{\alpha n} + a_{n-1} s^{\alpha n-1} + \cdots + a_0 s^{\alpha_0}} \quad (7) $$

Authorized licensed use limited to: Queen Mary University of London. Downloaded on November 05,2020 at 13:08:23 UTC from IEEE Xplore. Restrictions apply.

B. *Fractional Order PID Controller*

In time domain the control low of FOPID controller define as following:

$$u(t) = K_p.e(t) + K_i.\int_t^{\lambda} e(t) + K_d.D_t^{-\alpha}e(t) \quad (8)$$

Where the integral and derivative components are λ and μ respectively. Error signal is $e(t)$ and the fractional order signal is define as $\int_t^{\alpha} x(t) = \mathfrak{D}_t^{-\alpha}x(t)$. The parallel form transfer function in Laplace domain is the following:

$$C(s) = K_p + \frac{K_i}{s^{\lambda}} + K_d.s^{\lambda} \ , \ \lambda, \mu \epsilon (0,2) \quad (9)$$

FOPID controller has five adjustable control parameters K_p, K_i, K_d,λ,μ. Therefore, in comparison with classical PID controller which has only three adjustable parameters K_p, K_i, K_d, the FOPID controller has more ability. With respect to the lambda and gamma values in Eq (9), it can be found that the traditional PID controller is a special case of FOPID controller. In Fig 2 this cases are denoted.

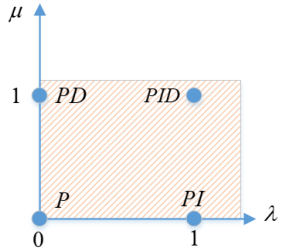

Figure 2. Different case of fractional order PID controller

IV. Distibuted Average Consensus Protocol

In proposed distributed strategy each of ES systems has average state estimator. In another world this state estimator use of the local information and measurement from the neighboring ES systems. Then use of them to update the local estimate of average ES system per-unit energy level $\overline{e_i}$ as well as average microgrid bus voltage $\overline{v_i}$. A distributed average consensus protocol implement in average state estimator for for tracking dynamic signals from [12].

Using a sparse communication graph $\mathcal{G}(\mathcal{V}, \mathcal{E})$, ES systems are connected together. Which $\mathcal{V} = \{1, \dots, N\}$ represent nodes and $\mathcal{E}$ is represent the edges. So that, nodes show the ES systems and edges show the communication link between them. If there is a direct communicate between the nodes, they are connected. To a certain number of nodes that are connected to node i, they are called the neighborhood of node i and are denoted by N_i. A diagonal matrix D represent the degree matrix of graph and its elements are d_i , which $d_i = |N_i|$. The matrix A denote the adjacency matrix of the graph and defined by $a_{ij} = 1$ if and only if $(i,j)\epsilon\mathcal{E}$, and $a_{ij} = 0$ otherwise. The Laplacian matrix of graph denoted by $L = D - A$. In undirected graphs, the Laplacian matrix has a single zero eigenvalue as well as another eigenvalues have greater value of zero $0 = \lambda_1(L) < \lambda_2(L) \leq \dots \lambda_N(L)$.

The distributed average consensus protocol as following:

$$\overline{x}_i(t) = x_i(t) + \int \sum_{j\epsilon N_i} a_{ij}\left(\overline{x}_j - \overline{x}_i\right) \quad (10)$$

Therefore, For the $i-$th ES system, let x_i be a local state variable, and let $\overline{x}_i$ be the local estimate of the average value of that state for the microgrid ES systems. The i-th ES system receives average state estimates from its neighbors, and its average state estimator implements mentioned distributed average consensus protocol.

The global dynamics of the distributed average consensus protocol are given by:

$$\dot{\bar{\mathbf{x}}} = \dot{\mathbf{x}} - \mathbf{L}\bar{\mathbf{x}} \quad (11)$$

Where $\mathbf{x} = [x_1, x_2, \dots, x_N]$ and $\bar{\mathbf{x}} = [\bar{x}_1, \bar{x}_2, \dots, \bar{x}_N]$.

By converting Laplace from Eq (11), we come to the following equation:

$$\mathbf{H}^{\text{avg}} = \frac{\bar{\mathbf{X}}}{\mathbf{X}} = \mathrm{s}(\mathrm{s}\mathbf{I}_{\mathrm{N}} + \mathbf{L})^{-1} \quad (12)$$

Which represents transfer function matrix for the distributed average consensus protocol [12]. $\bar{\mathbf{X}}$ and $\mathbf{X}$ are the Laplace transforms of $\bar{\mathbf{x}}$ and $\mathbf{x}$, respectively. For a balanced communication graph with a spanning tree, the steady-state gain of the average consensus protocol is given by the averaging matrix [13]:

$$\lim_{s\to 0} \mathbf{H}^{avg} = \mathbf{Q}, where\ [\mathbf{Q}]_{ij} = \frac{1}{N} \quad (13)$$

The final value theorem shows that for a vector of step inputs, the elements of $\mathbf{x}$ converge to the global average of the steady-state values x^{ss}:

$$\lim_{t\to\infty} \bar{\mathbf{x}}(t) = \lim_{s\to 0} \mathbf{H}^{avg} \lim_{s\to 0} s\mathbf{X} = Q\,\mathbf{x}^{ss} = \langle \mathbf{x}^{ss} \rangle \underline{1} \quad (14)$$

V. Distibuted Control Strategy

To regulate the DC-DC converter output voltage a voltage-current droop control used as following:

$$v_i^* = v^{mg} - F_i r_i (i_i - u_i^{\overline{v}} - u_i^e) \quad (15)$$

Where , v^{mg} is microgrid voltage reference and i_i is locally measured output current. It is known from the equation (15), two extra control signals $u_i^{\overline{v}}$, u_i^e are added to droop equation. $u_i^{\overline{v}}$ is voltage stabilization control signal and u_i^e is power sharing control signal. They are defined to balance the energy level between the ES systems and to maintain it through the load sharing and regulate the average microgrid bus voltage.

In order to use the maximum capacity of the ES systems to maintain the microgrid voltage with maximum deviation from Δv the microgrid reference, the virtual resistance is designed as following:

$$r_i = \frac{\Delta v}{\frac{P_i^{max}}{v^{mg}}} \quad (16)$$

In decentralized drop control, the load is usually divided by the inverse ratio of the virtual resistance r_i in the ES systems. The DC microgrid have high frequency harmonics for the switching of converters. To avoid the high frequencies, a low-pass filter is used with cut-off frequency of ω_i^c.

$$F_i = \frac{\omega_i^c}{s + \omega_i^c} \quad (17)$$

The current regulation is done in two stage [14].

Authorized licensed use limited to: Queen Mary University of London. Downloaded on November 05,2020 at 13:08:23 UTC from IEEE Xplore. Restrictions apply.

A proportional-integral (PI) voltage controller G_i^v at the first stage design as following:

$$i_i^* = G_i^v(v_i^* - v_i), G_i^v = p_i^{vp} + \frac{p_i^{vi}}{s} \quad (18)$$

This controller defined to set the converter current reference to regulate the output voltage of the ES system. At the second stage the current controller sets the duty cycle of the PWM switching to control the bipolar junction transistors (BJTs) of the converter, and to regulate the output current. For power sharing control signal u_i^e applied a fractional PI controller in (19) to set the energy level e_i to the local estimate of the average energy level of ES systems. Due to the difference between the capacities of energy storage systems, the per-unit energy level is used for power sharing balance.

$$u_i^e = G_i^e(e_i - \overline{e_i}), G_i^e = p_i^{ep} + \frac{p_i^{ei}}{s^\lambda} \quad (19)$$

Moreover, for voltage stabilization control signal $u_i^{\bar{v}}$ applied a fractional PI controller in (20) to voltage regulation of the microgrid, where the local estimate of the average bus voltage is regulated to the voltage reference of the microgrid.

$$u_i^{\bar{v}} = G_i^{\bar{v}}(v^{mg} - \overline{v_i}), G_i^{\bar{v}} = p_i^{\bar{v}p} + \frac{p_i^{\bar{v}i}}{s^{\lambda\_\bar{v}}} \quad (20)$$

A block diagram of control strategy is shown in Fig 3.

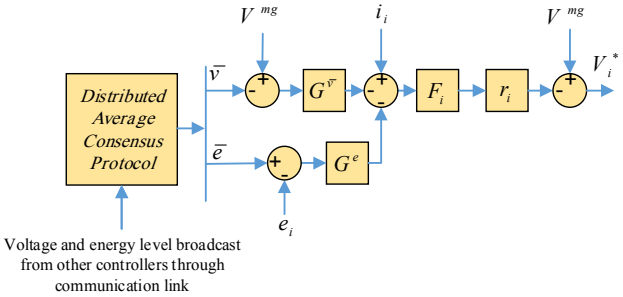

Figure 3. Control strategy

DC - DC converters operate at a high switching frequency with a switching period delay (T_s). The used DC-DC converter shown in Fig 4.

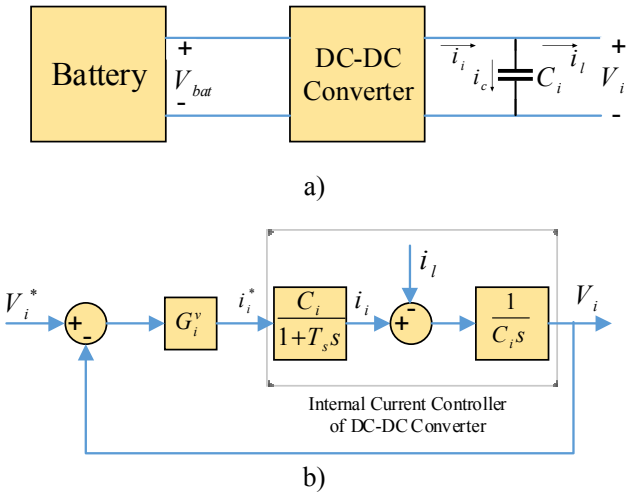

Figure 4. Model of the DC-DC converter and its controller: (a) DC-DC converter circuit; (b) block diagram of the local converter controller.

To design the external loop control, the closed loop voltage regulation dynamic between the output voltage reference of the ES system and the local bus voltage can be modeled by the following transfer function [15].

$$H_i^{v_{cl}} = \frac{H_i^{v_{ol}}}{1+H_i^{v_{ol}}}, \text{ where } H_i^{v_{ol}} = \frac{G_i^v}{sC_i(T_s s+1)} \quad (21)$$

Therefore, the dynamic balancing of the local bus voltage of the microgrid is obtain as:

$$\mathbf{V} = \mathbf{H}^{v_{cl}}\mathbf{V}^*, \text{ where } \mathbf{H}^{v_{cl}} = \text{diag}\{H_i^{v_{cl}}\} \quad (22)$$

The bus voltage and ES systems output current are related to each other using the admittance matrix.

$$\mathbf{I} = \mathbf{YV} \quad (23)$$

The admittance matrix is obtained using the impedance of the lines and loads. The first-order model is used for batteries energy level dynamic [15].

$$\dot{e}_i = -\frac{v_i i_i}{e_i^{max}} \quad (24)$$

Where e_i^{max} is the maximum energy capacity of i-th ES system. The global energy dynamics is following:

$$\mathbf{E} = \mathbf{MYV}, \mathbf{M} = diag\{-\frac{v^{mg}}{e_i^{max}{}_s}\} \quad (25)$$

The global closed-loop voltage regulation dynamics by multiple output linear system can be described as follow:

$$\mathbf{V} = \left[\left((\mathbf{H}^{vcl})\right)^{-1} + \mathbf{FrG}^{\bar{v}}\mathbf{G}^{avg} - \mathbf{FrG}^{e}(\mathbf{I}_N - \mathbf{G}^{avg})\mathbf{MY}\right]^{-1} V^{mg}(\mathbf{I}_N + \mathbf{FrG}^{\bar{v}})\underline{1} \quad (26)$$

VI. Case Study DC Microgrid

The case study DC microgrid have shown in Fig 5. This case study is 10 bus DC microgrid that have a PV as a distributed generation that connected to bus 1, 10 batteries as ES systems and 10 loads that each of them is connected to its bus. A 150 kW rated rectifier provides main grid connection of the microgrid at bus 1. The value of batteries capacity and loads provided in Table I. The loads connected to the buses of 1 to 5 are 15 kW and the loads connected to the busses 6 to 10 are 5 kW. The batteries capacity for buses 1 to 7 are 25kWh and for busses 8 to 10 are 12.5kWh. The PV generation with MPPT was simulated based on the modeling approach from [17]. PV irradiance data is shown in Fig 6. The battery ES systems are connected by a sparse communication network and this communication network are bidirectional. If there is connection link between the buses the elements a_{ij} of adjacency matrix are '1' and if there isn't connection link between the buses the elements a_{ij} of adjacency matrix are '0'.

Authorized licensed use limited to: Queen Mary University of London. Downloaded on November 05,2020 at 13:08:23 UTC from IEEE Xplore. Restrictions apply.

The communication link between ES systems are shown in Fig 5. Based on the analysis of conventional wiring configurations of the DC microgrids shown in [18] for data centers, $50m \times 24mm$ cables are selected to connect the load buses to bus 1.

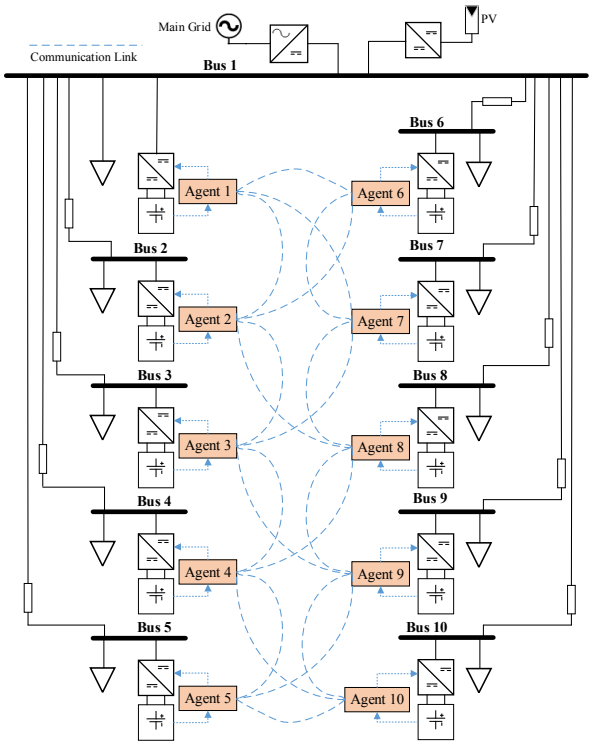

Figure 5. Model of the DC-DC converter and its controller.

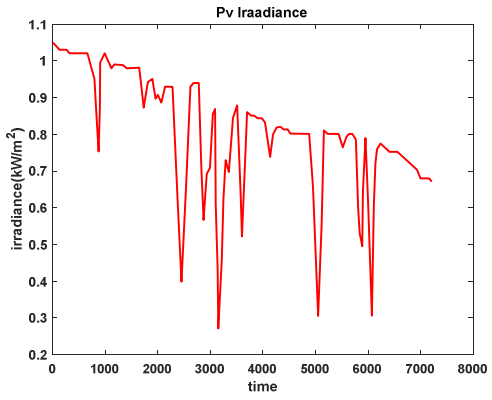

Figure 6. Data of the PV solar irradiance used in this case study.

Bus	Batteries Capacity	Load Power	Bus	Batteries Capacity	Load Power
Bus 1	25 kW	15 kW	Bus 6	25 kW	5 kW
Bus 2	25 kW	15 kW	Bus 7	25 kW	5 kW
Bus 3	25 kW	15 kW	Bus 8	12.5 kW	5 kW
Bus 4	25 kW	15 kW	Bus 9	12.5 kW	5 kW
Bus 5	25 kW	15 kW	Bus 10	12.5 kW	5 kW

Table I. Value of load and batteries capacity at each bus.

VII. Simulation Result

To simulate, we have considered a scenario. In this scenario, the PV power can be less than the power consumption of the microgrid (100 kW). In this case, the microgrid is connected to the main grid and receives the remaining power from the grid, hence we can verify the microgrid operation in both islanding and grid-connected mode. The parameters of simulation have shown in Table II.

As indicated from Fig 7, the voltage of each bus at less than 20 s converges to the microgrid reference voltage 380 V. When the power of PV is less than 100 kW, there is a very slight variation in the voltage of buses, after that they converge to the microgrid reference voltage 380 V. The variation value is less than 0.5 V and this indicates the performance of the used algorithm.

In Fig 8, the energy level of the ES systems is shown. As it is known that in less than 1 second, each ES system runs from their initial values to the value of 1 and charge completely. When the PV power is less than 100 kW, the batteries supply the power required loads and save the balancing voltage of the buses. Also, the convergence of the per-unit energy level ES systems have a per-unit energy level in each step of the scenario.

In Fig 9, the voltage deviation of each bus is shown. As it is clear that at all times of operation, the voltage deviation does not exceed 0.5 V. In designing the virtual resistance value, we set the voltage deviation value equal to 3% which is equal to 11.4 volts for the 380 V microgrid. With the proposed control strategy, the voltage deviation of each bus is much lower than the allowable value of voltage deviation. This is for good performance of the proposed control strategy.

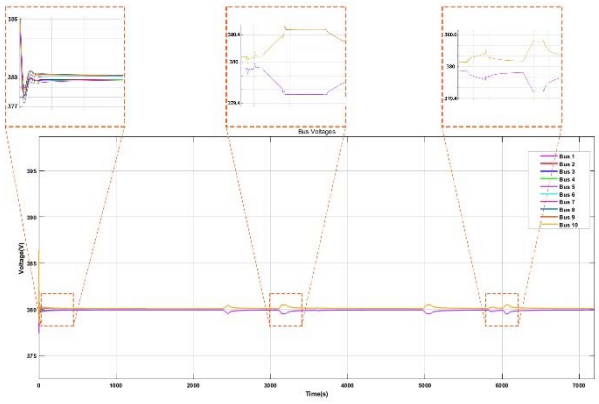

Figure 7. Voltage of buses under proposed strategy.

R_{dc}	36mΩ	p_i^{vp}	10	λ_e	0.7
L_{dc}	7μH	p_i^{vi}	10	$p_i^{\bar{v}p}$	5
$r_{1\text{-}5}$	0.2786	ω_i^c	100 rad/s	$p_i^{\bar{v}i}$	20
$r_{6\text{-}10}$	0.8365	p_i^{ep}	50	λ_v	1.5
Voltage	380	p_i^{ei}	100		

Table II. Simulation Parameters.

Authorized licensed use limited to: Queen Mary University of London. Downloaded on November 05,2020 at 13:08:23 UTC from IEEE Xplore. Restrictions apply.

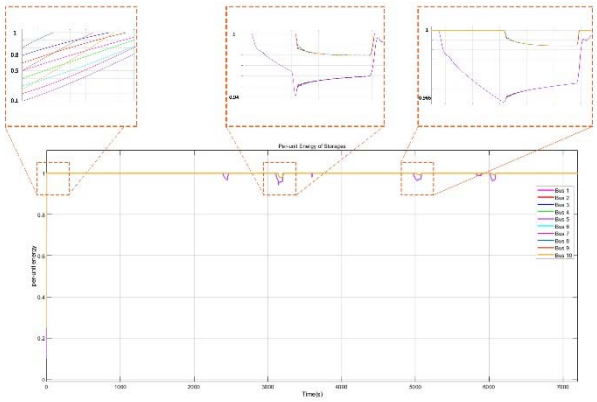

Figure 8. Per-unit energy level of ES systems.

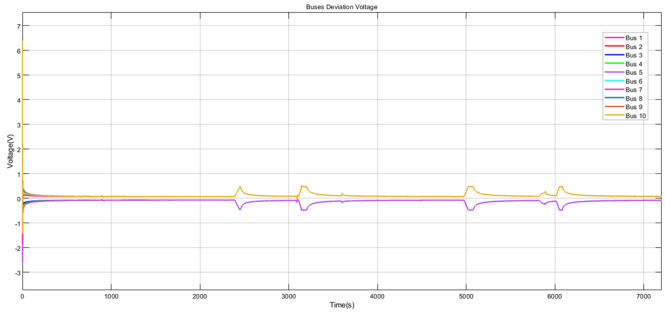

Figure 9. Deviation Voltage of buses from 380 V reference.

VIII. CONCLUSION

This investigation has thoroughly presented the design and performance evaluation of a novel distributed control strategy with fractional PI controller. The objective of this strategy is to stabilize the voltage of the microgrid buses at a reference value of 380 volts that are carried out by the DC output voltage control of the DC-DC converters. The controller has the ability to balance the energy level of the ES systems and the microgrid output voltage regulation. The fractional order controllers perform well in this strategy. The speed of voltage and the energy level convergence against the changes from islanding mode to grid-connected mode are the properties of these controllers and this is because of the higher degree of freedom of these controllers than traditional PI controllers. Simulation results show well the performance of this control strategy. The stabilization of the microgrid voltage and low voltage deviation against the mode changes as well as the balance at the energy level of the ES systems is the advantages of this strategy.

REFERENCES

[1] D. Chen and L. Xu, "Autonomous DC voltage control of a DC microgrid with multiple slack terminals," *IEEE Trans. Power Syst.*, vol. 27, no. 4, pp. 1897–1905, 2012.

[2] A. M. E. I. Mohamad and Y. A.-R. I. Mohamed, "Investigation and Assessment of Stabilization Solutions for DC Microgrid With Dynamic Loads," *IEEE Trans. Smart Grid*, vol. 10, no. 5, pp. 5735–5747, 2019.

[3] T. Samad and A. M. Annaswamy, "Controls for Smart Grids: Architectures and Applications," *Proc. IEEE*, vol. 105, no. 11, pp. 2244–2261, 2017.

[4] S. A. Alavi, K. Mehran, Y. Hao, A. Rahimian, H. Mirsaeedi, and V. Vahidinasab, "A distributed event-triggered control strategy for dc microgrids based on publish-subscribe model over industrial wireless sensor networks," *IEEE Trans. Smart Grid*, vol. 10, no. 4, pp. 4323–4337, 2019.

[5] F. L. Lewis, H. Zhang, K. Hengster-Movric, and A. Das, *Cooperative Control of Multi-Agent Systems: Optimal and Adaptive Design Approach*, vol. 53, no. 9. 2014.

[6] T. Morstyn, B. Hredzak, and V. G. Agelidis, "Control Strategies for Microgrids with Distributed Energy Storage Systems: An Overview," IEEE Trans. Smart Grid, vol. 9, no. 4, pp. 3652–3666, 2018.

[7] T. Morstyn *et al.*, "Unified Distributed Control for DC Microgrid Operating Modes," pp. 1–11, 2015.

[8] Y. Chen and I. Petr, "Fractional Order Control - A Tutorial," pp. 1397–1411, 2009.

[9] C. A. Monje, Y. Chen, B. Vinagre, D. Xue, and V. Feliu, *Fractional-Order Systems and Controls: Fundamentals and Applications*, ser. Advances in Industrial Control. Springer Verlag, 2010.

[10] Tepljakov, A., Alagoz, B. B., Yeroglu, C., Gonzalez, E., HosseinNia, S. H., & Petlenkov, E. (2018). FOPID controllers and their industrial applications: A sur- vey of recent results. *IFAC-PapersOnLine, 51* (4), 25–30.

[11] S. Dadras and H. R. Momeni, "Control of a fractional-order economical system via sliding mode," *Physica A*, vol. 389, no. 12, pp. 2434–2442, 2010.

[12] D. P. Spanos, R. Olfati-saber, and R. M. Murray, "Dynamic consensus for mobile networks," in 16th Int. Fed. Aut. Control (IFAC), 2005, pp. 1–6

[13] V. Nasirian, S. Member, S. Moayedi, S. Member, and A. Davoudi, "Distributed Cooperative Control of DC Microgrids," vol. 8993, no. c, pp. 1–29, 2014.

[14] J. Mayo-Maldonado, R. Salas-Cabrera, J. Rosas-Caro, J. De Leon-Morales, and E. Salas-Cabrera, "Modelling and control of a DCDC multilevel boost converter," IET Power Electronics, vol. 4, no. 6, p. 693, 2011.

[15] D. Chen, L. Xu, and L. Yao, "DC network stability and dynamic analysisusing virtual impedance method," in Proc. 38th Annual Conf. IEEE Ind. Electron. Soc. (IECON 2012), Oct. 2012, pp. 5625–5630.

[16] K. Le Dinh and Y. Hayashi, "Coordinated BESS control for improving voltage stability of a PV-supplied microgrid," in Proc. 2013 48th Int. Universities' Power Engineering Conf. (UPEC), Sep. 2013, pp. 1–6.

[17] M. G. Villalva, J. R. Gazoli, and E. R. Filho, "Comprehensive approach to modeling and simulation of photovoltaic arrays," IEEE Trans. Power Electronics, vol. 24, no. 5, pp. 1198–1208, May 2009.

[18] T. Tanaka, K. Hirose, D. Marquet, M. Szpek, E. S. Laboratories, and F. T. Orange, "Analysis of Wiring Design for 380-VDC Power Distribution System at Telecommunication Sites," pp. 1–5, 2012.

Authorized licensed use limited to: Queen Mary University of London. Downloaded on November 05,2020 at 13:08:23 UTC from IEEE Xplore. Restrictions apply.